

Affinity-based constraint optimization for nearly-automatic vessel segmentation

O. Cooper^a and M. Freiman^a and L. Joskowicz^a and D. Lischinski^a

^aSchool of Engineering and Computer Science, The Hebrew University of Jerusalem, Israel.

ABSTRACT

We present an affinity-based optimization method for nearly-automatic vessels segmentation in CTA scans. The desired segmentation is modeled as a function that minimizes a quadratic affinity-based functional. The functional incorporates intensity and geometrical vessel shape information and a smoothing constraint. Given a few user-defined seeds, the minimum of the functional is obtained by solving a single set of linear equations. The binary segmentation is then obtained by applying a user-selected threshold. The advantages of our method are that it requires fewer initialization seeds, is robust, and yields better results than existing graph-based interactive segmentation methods. Experimental results on 20 vessel segments including the carotid arteries bifurcation and noisy parts of the carotid yield a mean symmetric surface error of 0.54mm (std=0.28).

Keywords: Vessels segmentation, optimization

1. INTRODUCTION

Vessel segmentation from medical CTA images is a clinical routine for many diagnostic and surgical applications. The segmentation is useful to understand the spatial structure of the vessels and bifurcation, to measure the vessels dimensions and associated pathologies such as stenosis and aneurisms, and to plan interventional radiology procedures, such as catheter insertion, and stent and balloon placement.

A variety of vascular structure segmentation techniques have been developed in the past decade.¹ They include geometric shape,² intensity values,³ active contours,^{4,5} statistical active shape models,⁶ and contour tracking⁷⁻⁹ techniques. Automatic and semi-automatic segmentation techniques frequently miss vessel segments and small vessels altogether, report inaccurate vessel diameters, include spurious anatomical structures, and fail on bifurcation and pathologies. The failures are often due to the intrinsic vessels characteristics and differences in the various regions of the body. Consequently, interactive tools are required to correct such segmentation flaws. Interactive vessel segmentation methods should be simple, generic, robust, accurate, and intuitive to use, so that the treating physician can produce and correct a vasculature segmentation in a few minutes.

2. RELATED WORK

Recently developed methods can be classified into three main categories: 1) region growing,¹⁰ 2) fast marching and level-sets,¹¹ and 3) tracking methods.⁷ Most methods require extensive user interaction and the adjustment of non-intuitive parameters, which make their clinical use impractical.

Region growing techniques start at an initial seed and iteratively add voxels on the region border based on a predefined criterion. The criterion to add to the region is usually based on the voxel's intensity, i.e., a predefined similarity threshold, or computed by a dynamic estimation algorithm. These methods often yield over-segmentation and segmentations with artificial segmentation holes due to image noise and variance of the voxels' intensities across regions.

Level sets methods evolve a front from one or more seed points towards the object's boundary. The front is implicitly defined as the zero level set of a function, and is evolved in its local normal direction. Representing the front as the zero set of a function has the advantage that topological changes in the front are explicitly handled. The front evolution is determined by the normal front direction at each point and by the local speed

Further author information: Send correspondence to M. Freiman at freiman@cs.huji.ac.il
Other emails: ofr.cooper@gmail.com, josko@cs.huji.ac.il, danix@cs.huji.ac.il

at which the front expands. The front propagation speed is determined locally from the front curvature. The proper choice of the function expansion speed is critical, as it influences the convergence speed, accuracy, and other factors.¹¹ The main drawbacks of these methods is that they require laborious parameter tuning and are very time consuming.

Tracking methods follow the central axis of a vessel starting from a user-specified seed point. The central axis is tracked by propagating a front wave with level-set methods, or by advancing it in the direction of the vessel from the current endpoint. In most cases, assumptions about the shape and size of vessels must be incorporated, for otherwise the segmentation “leaks” to nearby tissues in areas of low contrast. The main drawback of these methods is that they do not handle well vessel irregularities that have not been predefined in their shape models.

Graph-based interactive segmentation methods^{12,13} are general and have shown promise in a variety of segmentation tasks. The min-cut approach¹² is based on the construction of object/background models starting from user-defined seeds and solving the corresponding min-cut problem. Since the algorithm computes the smallest cut separating the given seeds, it often produces the cut that minimally separates the seeds from the rest of the image. Consequently, additional interaction is required to reconnect them and to ensure the connectivity of the segmented vessels.

Grady’s random-walk distance-based algorithm¹³ provides a natural multiple object segmentation for user-defined seeds for each label. The algorithm labels the remaining pixels based on its estimated distance from the seeds by resolving the question: given a random walker starting at this location, what is the probability that it reaches each of the seed points. The final segmentation is computed by assigning the label with the highest probability to each voxel. The probability for each label is computed by solving a set of linear equations. Since the probabilities are computed independently at each voxel, and only the label with the maximal probability is chosen at each voxel without considering its local neighborhood, the solution may lead to an erroneous segmentation, where a single voxel is marked differently from its local environment.

In this paper we describe a new interactive segmentation tool for vessel segmentation. It extends the optimization framework proposed by Levin et al.¹⁴ for colorization of 2D grayscale images for the segmentation of 2D and 3D images by incorporating geometric shape prior information. Unlike the graph-cut¹² method, our method ensures the connectivity of the segmented object and does not require the estimation of the object/background models. Only a few user seeds are required. Our method provides soft (continuous) segmentation of an image by solving a single set of linear equations. A binary segmentation is then obtained by applying a user-specified threshold. Since each voxel’s local neighborhood contributes to its marking in the segmentation, our method yields more accurate segmentations than those of the random-walk method.¹³ Experimental results on vascular image segmentation from 20 clinical CTA images confirms that our method is fast, robust, accurate, practical, and can be used by non-technical users.

3. METHOD

Our method produces a continuous segmentation map based on the original image, a few user-specified seeds, and thresholds for background and object structures. The algorithm propagates the seeds throughout the image, taking into account the affinity between voxels as calculated from their intensity and from the spatial shape information. The output is a map that indicates the affinity of each voxel to the original seeds. The user can then select an appropriate threshold to obtain a binary segmentation.

To constitute a satisfactory segmentation, the propagation result should fulfill two requirements:

1. Satisfy the user-specified constraints as closely as possible, as required in scattered data approximation problems.
2. Be as smooth as possible, as unnecessary propagation oscillations will result in noisy segmentation. Rapid changes in the propagation should be allowed, however, across significant edges in the image, with the rate of change in the propagation being commensurate with the rate of change in input intensity at each voxel.

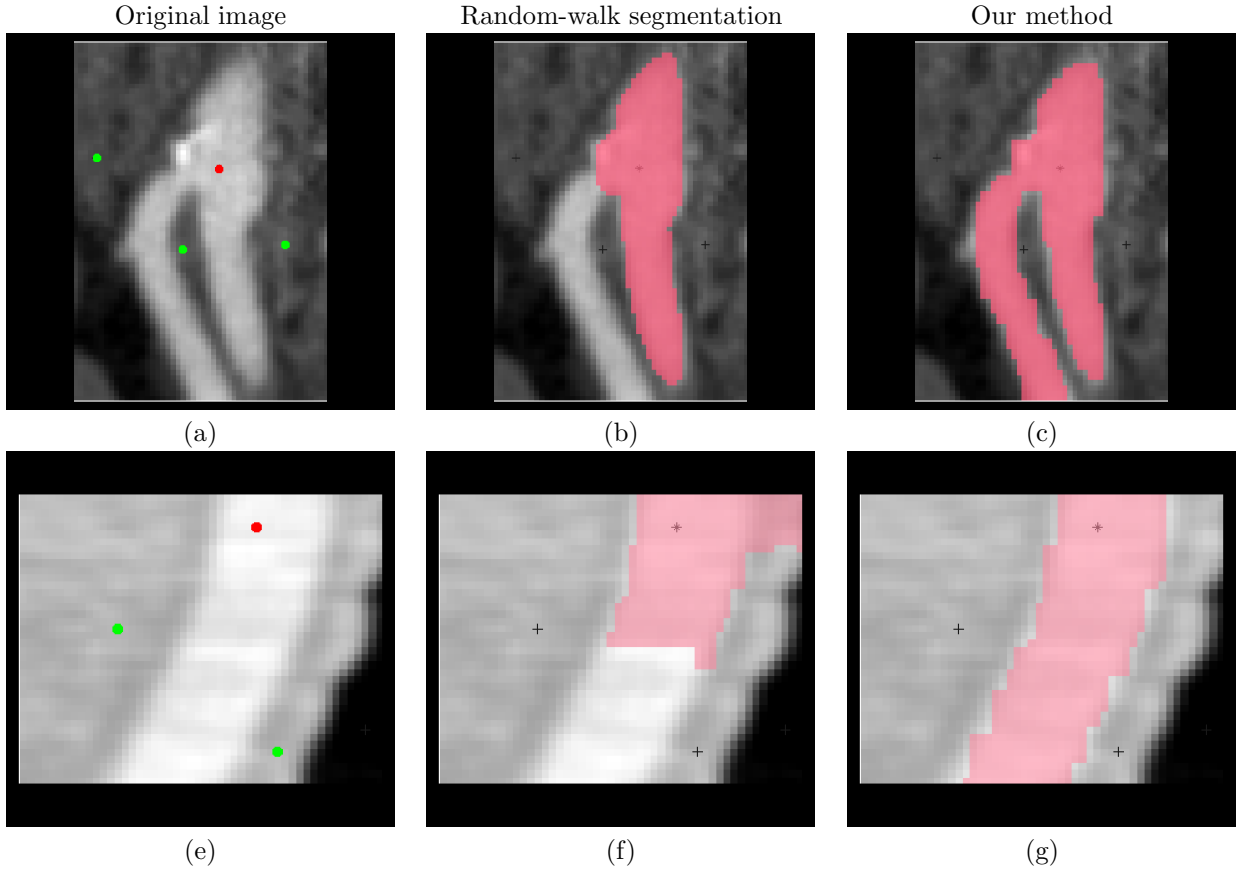


Figure 1. Segmentation results of two vessel segments: (a) and (d) show the CTA vessel segments with the object seed (red) and background seeds (green); (b) and (e) show the random-walk¹³ segmentation results; (c) and (f) show our method results.

To achieve these objectives, we seek a function f that minimizes the quadratic energy functional:

$$f = \operatorname{argmin}_f \left(\sum_{\vec{x}} w(\vec{x})(f(\vec{x}) - g(\vec{x}))^2 + \lambda \sum_{\vec{x}} h(\nabla f, \nabla L) \right) \quad (1)$$

where \vec{x} is the coordinate vector for the image voxels, g is the image of the user's seeds, L is the log of the input image, and $w(\vec{x})$ is a binary function whose value is 1 for voxels that were marked by the user and 0 otherwise.

The first term in the functional is the data term that enforces the user-specified non-overlapping constraints. The second term is the smoothing (regularization) term, whose objective is to keep the gradients of the segmentation function f as small as possible, except where the underlying image has significant gradients in its log-intensity channel L . We use the log-intensity to make the results independent of the overall brightness of the image. This is achieved because only the gradients of the image are considered in the equation, and if the image is multiplied by a constant (which corresponds to brightness amplification), the gradients of the logarithm of the image do not change. Following Lischinski et al.,¹⁵ we define the smoothing term h as:

$$h(\nabla f, \nabla L) = \frac{|f_x|^2}{|L_x|^{\alpha + \varepsilon}} + \frac{|f_y|^2}{|L_y|^{\alpha + \varepsilon}} + \frac{|f_z|^2}{|L_z|^{\alpha + \varepsilon}} \quad (2)$$

where subscripts x, y, z denote the spatial differentiation of the functions f and L , the exponent α controls the sensitivity of the term to the derivatives of the log-input image, and ε is a small constant to avoid division by zero and reduce the effect of image noise on h . The relative weight of the two terms in the functional is controlled by the parameter λ .

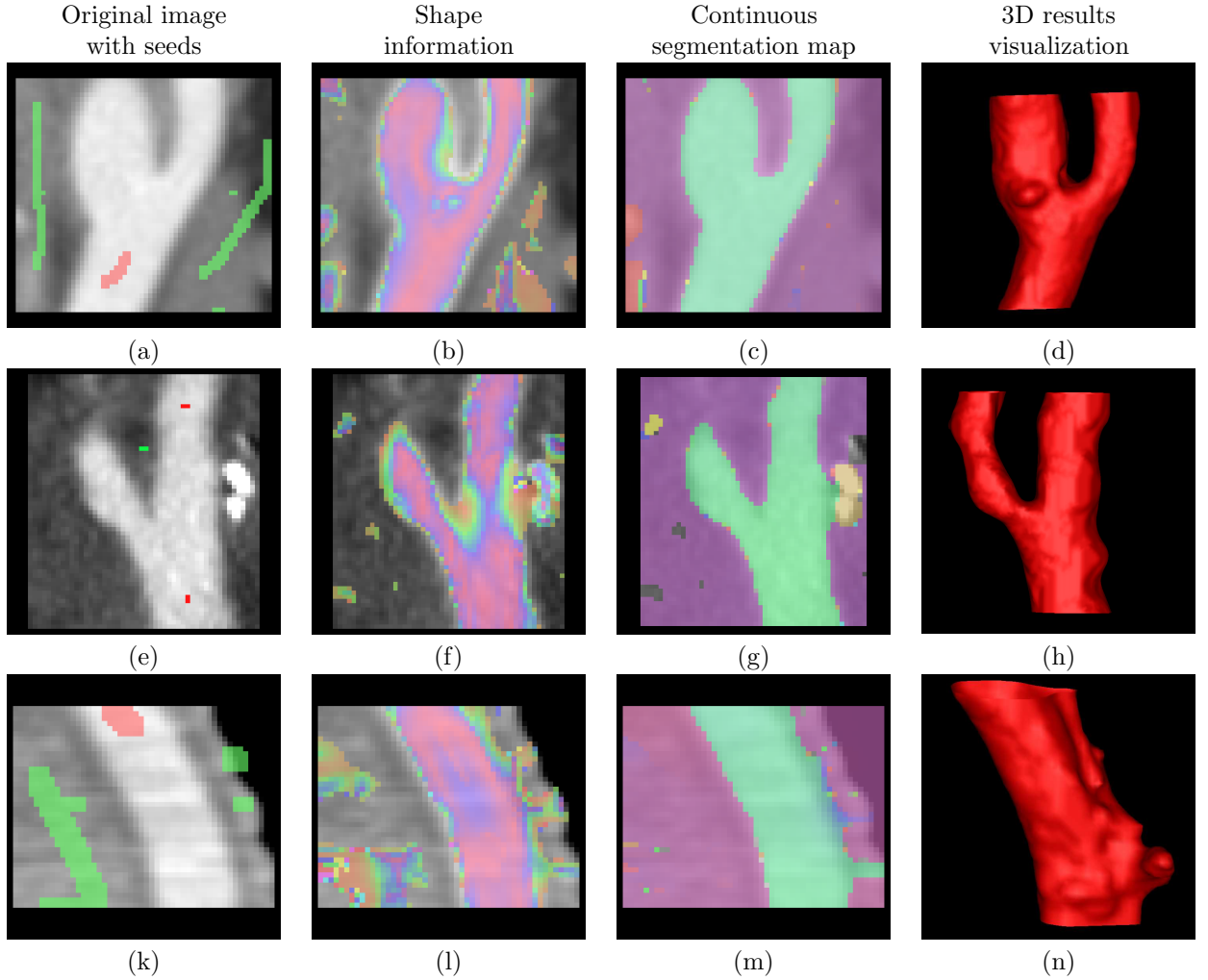


Figure 2. Illustration of the segmentation process and its results for three carotid artery segments. The first and second rows show carotid artery bifurcation segments; the third is a carotid segment from a noisy image. The first column (a, e, k) shows the original CTA images with user seeds (object seeds are red, background seeds are green). The second column (b,d,l) shows the vesselness map overlaid on the original image (red pixels indicate high vesselness values). The third column (c,g,m) shows the continuous segmentation map overlaid on the original image. The last column (d,h,n) shows 3D visualizations of the segmented vessel surfaces.

Using standard finite differences for the spatial derivatives of f results in a quadratic expression in f whose unique minimum is obtained by solving the linear system:

$$Af = b \quad (3)$$

where

$$A_{i,j} = \begin{cases} -\lambda (|L_i - L_j|^\alpha + \varepsilon)^{-1} & j \text{ is a neighbor of } i (j \sim i) \\ w_i - \sum_k A_{i,k} & i = j \text{ and } k \text{ is neighbor of } i \\ 0 & \text{otherwise} \end{cases} \quad (4)$$

$$b_i = w_i g_i \quad (5)$$

Subscripts i and j denote image voxels.

Solving this linear equation system using a direct solver is not feasible, as the matrix A is very large and solving for it requires more memory than is available in most computing environments. However, since the matrix A is a sparse, symmetric, and positive-definite matrix, iterative solvers are effective in solving the linear problem. We will prove it is a positive-definite matrix by directly examining the quadratic expression $x^T Ax$, and in order to simplify the notation we introduce 2 new matrices, W and K , such that $A = W + K$. $W = \text{diag}(w_1, w_2, \dots, w_n)$ is a diagonal matrix, with the vector w as the diagonal, and K is a non-homogeneous laplacian matrix. To prove that A is positive definite, we show that $\forall \vec{x} \neq \vec{0}$, $x^T Ax > 0$. In the following equations, i and j are image pixels, and $i \sim j$ denotes spatial proximity between pixels i and j .

$$x^T W x = \sum_{i,j} x_i W_{i,j} x_j = \sum_i w_i x_i^2 \geq 0 \quad (6)$$

$$\begin{aligned} x^T K x &= \sum_{i,j} x_i x_j K_{i,j} = \sum_i x_i^2 K_{i,i} + \sum_{i,j \sim i} x_i x_j K_{i,j} = \\ &= \sum_i \sum_{j \sim i} -x_i^2 K_{i,j} + \sum_{i,j \sim i} x_i x_j K_{i,j} = \\ &= \sum_{i,j \sim i} -x_i^2 K_{i,j} + x_i x_j K_{i,j} = \\ &= \sum_{i,j \sim i, j > i} x_i x_j K_{i,j} + x_j x_i K_{j,i} - x_i^2 K_{i,j} - x_j^2 K_{j,i} = \\ &= \sum_{i,j \sim i, j > i} -K_{i,j} (x_i^2 + x_j^2 - 2x_i x_j) = \\ &= \sum_{i,j \sim i, j > i} -K_{i,j} (x_i - x_j)^2 \geq 0 \end{aligned} \quad (7)$$

$$x^T A x = x^T (W + K) x = x^T W x + x^T K x > 0 \quad (8)$$

In equations (6), (7) the inequality is true because every term in the final summation is non-negative. Equation (8) is true because (6) and (7) cannot be both equal to 0 at the same time. We show this by way of contradiction. Assume that (7) is zero. This implies that $x_i = x_j$ for all pixels i, j which are neighbors. So x is a constant non-zero vector, as every pixel equals its neighbors. In this case (6) must be strictly greater than 0, because there must be at least one w_i which is non-zero. If all w_i are 0, this means that the user made no markings on the image, and this we do not allow. This concludes the proof that A is a sparse positive-definite matrix.

The conjugate gradients algorithm with no preconditioner adequately solves the resulting equation system in near real time. Alternatively, a multi-grid approach such as those used by by Lischinski et al.¹⁵ and by Grady,¹⁶ can be used to speed up the computation.

3.1 Geometrical information incorporation

Since the vessel has a relatively well-defined tube-like shape, it is beneficial to incorporate this knowledge into our framework. First, the geometrical information is computed from the eigenvalues of the Hessian matrix using Frangi's formulation¹⁷ :

$$V(\sigma) = \begin{cases} 0 & \lambda_2 > 0 \text{ or} \\ & \lambda_3 > 0, \\ \left(1 - \exp\left(-\frac{R_A^2}{(2a)^2}\right)\right) \left(\exp\left(-\frac{R_B^2}{(2b)^2}\right)\right) \left(1 - \exp\left(-\frac{S^2}{(2c)^2}\right)\right) & \text{otherwise} \end{cases} \quad (9)$$

where

$$R_A = \frac{|\lambda_2|}{|\lambda_3|} \quad R_B = \frac{|\lambda_1|}{\sqrt{|\lambda_2 \lambda_3|}} \quad S = \sqrt{\lambda_1^2 + \lambda_2^2 + \lambda_3^2}$$

where $|\lambda_1| \leq |\lambda_2| \leq |\lambda_3|$ are the eigenvalues of the Hessian matrix and σ is the scale at which the measure is computed. In a tubular structure, λ_1 is very small, and λ_2 and λ_3 are of a large magnitude and identical sign. Frangi used these characteristics to define three measures: R_A differentiates between plate and line-like structures, R_B measures the deviation from blob-like structures, and S differentiates between foreground (vessel) and background (noise). Constants a , b and c are predefined weights determining the influence of R_A , R_B and S . The vesselness measure value is close to 1 for voxels with tube-like structures, and close to 0 otherwise. This value is computed at several scales and the maximum over all scales is taken for each voxel.

The functional is thus:

$$f = \underset{f}{\operatorname{argmin}} \left(\sum_{\vec{x}} w(\vec{x})(f(\vec{x}) - g(\vec{x}))^2 + \lambda \sum_{\vec{x}} h(\nabla f, \nabla L(V)) \right) \quad (10)$$

where L now is the log of the vesselness measure map V , as computed by (9).

The result is a vesselness measure map of the original data. We then use this image as input to the optimization framework, instead of the original grayscale CTA image. Fig. 2 illustrates the segmentation process on clinical CTA vessel images.

4. EXPERIMENTAL RESULTS

We evaluated the performance of our segmentation method on 20 clinically relevant carotid artery segments extracted from 10 clinical CTA datasets with resolution of $512 \times 512 \times 800$ voxels of size $0.5 \times 0.5 \times 0.55 \text{mm}^3$. Patients were administered 100cc of non-iodinated contrast agent by rapid injection at 3-4cc/sec. Difficult datasets were purposely selected to include various levels of stenosis and dental implants streaking artifacts. The vessel segments include the carotid artery bifurcation, and the lower part of the common carotid near the aortic arch, which is a very noisy region in the CTA image. Ground-truth segmentations of these vessel segments were obtained manually by a 3D segmentation expert and were validated by an expert radiologist.

For each vessel segment, we manually chose initialization seeds for the vessel and the background. In all cases, the extent of the user intervention did not exceed 3-4 mouse clicks. Empirically, we determined the values for λ to be between 1×10^{-5} and 1×10^{-6} , and the values for α between 3 and 10 and performed the segmentation. The user-specified threshold value was fixed for all of the experiments. The segmentation results of each region were evaluated following the methodology in¹⁸. Both volumetric and surface based measures were then computed. To evaluate the robustness of our method to seed location, we selected three different seeds for each vessel segment.

Table 1 summarizes the results for 20 segments for the different seeds and the difference between the three different seeds initializations for each segment. We focused on two particularly difficult regions: carotid bifurcations and poor contrast areas. The Average Symmetric Surface Distance (ASSD) compared to the ground-truth is 0.54mm, which is within the observer segmentation error range. The average ASSD difference between the three initializations is 0.24mm, which is about half the voxel size. The mean running time for each segment was 35.8sec (std=27.8) on standard dual-core 2.4GHz PC with 2Gb of memory. These results indicate that our method is accurate, easy to use and robust for different seeds selections. Therefore it can be used without extensive user training.

5. CONCLUSION

We have presented a new interactive method for vascular segmentation of CTA images. The method inputs a CTA image and a set of user-defined markings, and outputs a soft (continuous) segmentation, which can be turned into a binary segmentation by interactively selecting a threshold. The desired segmentation is modeled as a function that minimizes a quadratic affinity-based functional. The functional incorporates intensity and geometrical vessel shape information and a smoothing constraint. Given a few user-defined seeds, the minimum of the functional is obtained by solving a single set a sparse, symmetric, positive semi-definite system of linear equations.

	ASSD (mm)		RMS (mm)		MSSD (mm)		VOE	
	mean	std	mean	std	mean	std	mean	std
Carotid bifurcations	0.46	0.21	0.87	0.53	4.91	2.90	25.38	8.51
Poor contrast	0.67	0.31	1.12	0.59	6.37	3.57	32.25	8.52
Average	0.54	0.28	0.98	0.57	5.53	3.25	28.25	9.10

(a) Average segmentation results

	ASSD (mm)		RMS (mm)		MSSD (mm)		VOE (%)	
	mean	std	mean	std	mean	std	mean	std
Carotid bifurcations	0.18	0.18	0.43	0.47	2.28	2.57	4.21	3.53
Poor contrast	0.34	0.28	0.75	0.61	5.07	3.41	5.45	3.41
Average	0.24	0.23	0.56	0.55	3.45	3.19	4.73	3.44

(b) Sensitivity to seed selection

Table 1. Comparison metrics for the 20 test cases on two carotid artery segments: bifurcations and poor contrast regions. Table (a) shows the average discrepancy values compared to the ground-truth manual segmentation; Table (b) shows average differences of three initialization seeds. In both tables, First column indicates the vessel segment type. The second column is the Average Symmetric Surface Distance (ASSD) in mm. The third is the Root Mean Square Symmetric Surface Distance (RMS SSD) in mm. The fourth column is the Maximal Symmetric Surface Distance (MSSD) in mm, and the fifth is the Volumetric Overlap Error percentage (VOE) in %.

Our method requires only a few initialization seeds and a thresholding operation, and it is accurate, robust and intuitive to use. It incorporates both local and global intensity and shape information, and achieves better results compared to other graph-based interactive methods. Only two free parameters need to be specified, and in our experiments we have achieved good results on all cases for a small range of those parameters.

In the future, we plan to extend this method to other medical image segmentation tasks, including multi-organ segmentation, and to other structures, such as the brain and the liver.

Acknowledgments

This research was funded in part by a grant from the Israeli Ministry of Trade and Industry, MAGNETON Grant 38652.

REFERENCES

- [1] Kirbas, C. and Quek, F., “A review of vessel extraction techniques and algorithms,” *ACM Comput. Surv.* **36**(2), 81–121 (2004).
- [2] Frangi, A., Niessen, W., Vincken, K., and Viergever, M., “Multiscale vessel enhancement filtering,” in [*Proc. of the 1st Int. Conf. on Med. Image Comp. and Comp. Aided Interventions, MICCAI’98*], Wells, W.M. III, Colchester, A., and Delp, S., eds., *LNCS 1496*, 130–137 (1998).
- [3] Kim, D. and Park, J., “Connectivity-based local adaptive thresholding for carotid artery segmentation using MRA images,” *Image and Vision Comp.* **23**(14), 1277–1287 (2005).
- [4] Lorigo, L., Faugeras, O., Grimson, W., Keriven, R., Kikinis, R., Nabavi, A., and Westin, C., “Curves: Curve evolution for vessel segmentation,” *Med. Image Anal.* **5**, 195–206 (2001).
- [5] Nain, D., Yezzi, A., and Turk, G., “Vessel segmentation using a shape driven flow.,” in [*Proc. of the 7th Int. Conf. on Med. Image Comp. and Comp. Aided Interventions, MICCAI’04*], *LNCS 3216*, 51–59 (2004).
- [6] Lekadir, K., Merrifield, R., and Guang-Zhong, Y., “Outlier detection and handling for robust 3-D active shape models search,” *IEEE Trans. Med. Imaging* **26**(2), 212–222 (2007).
- [7] Schaap, M., Manniesing, R., Smal, I., Van Walsum, T., Van Der Lugt, A., and Niessen, W., “Bayesian tracking of tubular structures and its application to carotid arteries in CTA.,” in [*Proc. of the 10th Int. Conf. on Med. Image Comp. and Comp. Aided Interventions, MICCAI’07*], *LNCS 4792*, 562–570 (2007).
- [8] Manniesing, R., Viergever, M., and Niessen, W., “Vessel axis tracking using topology constrained surface evolution,” *IEEE Trans. Med. Imaging* **26**(3), 309–316 (2007).
- [9] Friman, O., Hindennach, M., and Peitgen, H.-O., “Template-based multiple hypotheses tracking of small vessels,” in [*Proc. of the 5th IEEE Int. Symp. on Biomedical Imaging: From Nano to Macro. ISBI’08.*], 1047–1050 (2008).
- [10] Bock, S., Kühnel, C., Boskamp, T., and Peitgen, H., “Robust vessel segmentation,” in [*Med. Imaging 2008: Computer-Aided Diagnosis*], **6915**, SPIE (2008).
- [11] Van Bommel, C., Spreuwers, L., Viergever, M., and Niessen, W., “Level-set based carotid artery segmentation for stenosis grading.,” in [*Proc. of the 5th Int. Conf. on Med. Image Comp. and Comp. Aided Interventions, MICCAI’02*], *LNCS 2489*, 36–43 (2002).
- [12] Boykov, Y. and Funka-Lea, G., “Graph cuts and efficient n-d image segmentation.,” *Int. J. of Comp. Vision* **70**(2), 109–131 (2006).
- [13] Grady, L., “Random walks for image segmentation,” *IEEE Trans. Patt. Anal. and Mach. Intell.* **28**(11), 1768–1783 (2006).
- [14] Levin, A., Lischinski, D., and Weiss, Y., “Colorization using optimization,” *ACM Trans. Graph.* **23**(3), 689–694 (2004).
- [15] Lischinski, D., Farbman, Z., Uyttendaele, M., and Szeliski, R., “Interactive local adjustment of tonal values,” in [*SIGGRAPH ’06: ACM SIGGRAPH 2006 Papers*], 646–653 (2006).
- [16] Grady, L., “A lattice-preserving multigrid method for solving the inhomogeneous poisson equations used in image analysis,” in [*Computer Vision – ECCV 2008*], Forsyth, D., Torr, P., and Zisserman, A., eds., *LNCS 5303*, 252–264, Springer (2008).
- [17] Frangi, A., Niessen, W., Koen, V., and Viergever, M., “Multiscale vessel enhancement filtering,” in [*Proc. of the 1st Int. Conf. on Med. Image Comp. and Comp. Aided Interventions, MICCAI’98*], *LNCS 1496*, 130–137 (1998).
- [18] Ginneken, B., Heimann, T., and Styner, M., “3D segmentation in the clinic: A grand challenge,” in [*3D Segmentation in the Clinic: A Grand Challenge*], Heimann, T., Styner, M., and van Ginneken, B., eds., 7–15. (2007). <http://www.sliver07.org>.